ACS OMEGA

http://pubs.acs.org/journal/acsodf

Article

Study on Overpressure Propagation Law of Vapor Cloud Explosion under Different Building Layouts

Minghua Chi, Hongye Jiang,* Xubin Lan, Taolong Xu, and Yi Jiang

Cite This: *ACS Omega* 2021, 6, 34003−34020

Read Online

ACCESS | Metrics & More | Article Recommendations

ABSTRACT: To determine and optimize the emergency evacuation path of personnel in the case of vapor cloud explosion caused by pipeline leakage and improve the safety control measures in the high-consequence areas of gas pipelines, this study was conducted. This work mainly studied two questions: whether various research methods applicable to the solid explosive explosion are also applicable to vapor cloud explosion and the influence of different building layouts on the overpressure propagation law of vapor cloud explosion. First, the applicability of several empirical models and computational fluid dynamics (CFD) methods in vapor cloud explosion overpressure prediction is systematically compared and analyzed. Second, the finite element models based on the fluid−structure interaction are established to study the overpressure propagation law under the influence of different building layouts. Finally, based on the overpressure propagation law, the determination and optimization principle of the emergency evacuation path of personnel when an accident occurs are given. The results show that the CFD method and empirical model based on equivalent assumption between trinitrotoluene and combustible gas are not suitable for the study of gas-phase explosion, while the mixed gas method based on CFD is more suitable for exploring the overpressure problem of vapor cloud explosion. Buildings arranged perpendicular to the direction of blast wave have the most obvious enhancement and weakening effect on overpressure, and the maximum increase rate and decrease rate are about 90%. The maximum increase rate of overpressure between two vertical layout buildings is more than 60% higher than that between two horizontal layout buildings. When determining the emergency evacuation path, the non-explosive side of the building perpendicular to the shock wave layout should be given priority. If it is necessary to pass through the building gap, the gap between the two horizontal layout buildings should be preferred to ensure that the damage of overpressure to personnel is minimized. The research results can provide a theoretical basis for the improvement of personnel safety control measures in high-consequence areas of the gas pipeline.

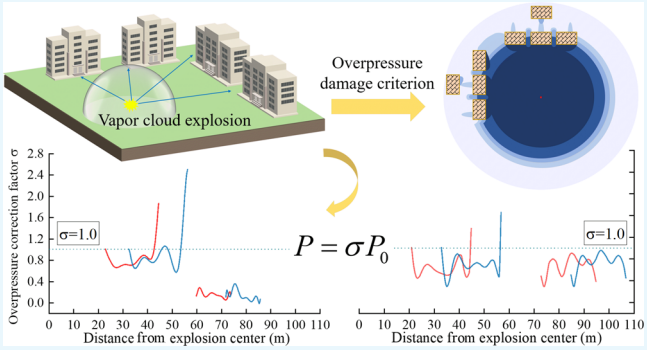

1. INTRODUCTION

As more and more gas pipelines are built and put into operation,[1] these pipelines will inevitably pass through specific areas, such as densely populated and densely built, forming new high-consequence areas or causing the upgrading of the original high-consequence areas.[2] Due to third-party damage, natural disasters, construction damage, or pipeline corrosion, the pipeline is prone to accidents such as small hole leakage, large hole leakage, and fracture.[3,4] Compared with the large hole and fracture leakage, the operation parameters of the pipeline are almost unaffected when the small hole leakage occurs. The characteristics of the leakage signal are not obvious and difficult to detect.[5] Once the gas pipeline leaks, a large number of natural gas leaks out and mixes with the air to form an explosive vapor cloud. When the vapor cloud explodes, people's life and property safety will be greatly damaged.[6,7] On July 2, 2017, a gas pipeline in Guizhou, China fractured and exploded, resulting in 8 deaths and 35 injuries. On June 13, 2021, an explosion accident of gas pipeline leakage occurred in a community in Hubei, China, resulting in 11 deaths and 37 injuries. Such accidents still happen.

In the event of an explosion accident, the surrounding buildings can be regarded as a large "explosion-proof wall" to some extent. The determination and optimization of the emergency evacuation path based on the building can effectively reduce the casualties caused by the accident. Given the harm caused by gas pipeline explosion accidents, scholars have conducted extensive research, and the research objects include

Received: September 26, 2021
Accepted: November 17, 2021
Published: November 30, 2021

adjacent parallel pipelines,[8,9] tunnels,[10] pipe corridors,[11] and buildings,[12] and so on. However, the influence of buildings on overpressure propagation has not been paid enough attention to in the high-consequence area of gas pipeline, especially in the multi-building area, and more attention is often paid to the influence of gas pipeline explosion on various engineering structures. At the same time, because vapor cloud explosion is essentially a gas explosion, whether the various research methods applicable to the solid explosive explosion are also applicable to vapor cloud explosion remains to be considered. Therefore, it is challenging to study the propagation law of vapor cloud explosion in gas pipelines under buildings. It is necessary to carry out a theoretical and systematic analysis of this series of problems to provide a theoretical basis for the determination and optimization of personnel safety evacuation routes, which is of great significance to the safety control of high-consequence areas of gas pipelines.

This work mainly studied the above two prominent problems: whether the research method suitable for the solid explosive explosion is suitable for vapor cloud explosion and the overpressure propagation law of vapor cloud explosion under different building layouts. First, the widely used explosion overpressure prediction methods were compared and analyzed, and the method suitable for analyzing the explosion overpressure of vapor cloud was selected. Second, according to the small hole leakage model, the scale of natural gas cloud formed by 1 and 2 h pipeline leakage was calculated. The finite element models based on the fluid-structure interaction (FSI) were established to analyze the state of building structure under extreme overpressure and the overpressure propagation law of the vapor cloud explosion under different building layout conditions. Third, the correction factor curves were fitted to simplify the process of peak overpressure prediction in practical engineering. Finally, the overpressure distribution of a typical population-intensive high-consequence area was analyzed, and the reference suggestions for determining the safety evacuation path were put forward to ensure the safety of personnel to the greatest extent when the vapor cloud explosion accident occurred.

2. THEORETICAL METHOD

2.1. Method Introduction. At present, there are mainly three kinds of research methods on the explosion problem: experiment, computational fluid dynamics (CFD) method, and empirical model. Due to the high cost and danger of experimenting. The CFD method and empirical model were used by most scholars. With the rapid development of computers, CFD has developed rapidly and has been widely used in oil and gas engineering,[13,14] aerospace engineering,[15] construction engineering,[16] bridge engineering,[17] and so on.[18] It has the characteristics of accurate calculation results; however, the CFD method requires high computational cost. In the study of the explosion problem, Yang[19] simulated the leakage explosion process of buried PE pipeline and analyzed the pressure and stress changes of pipeline and pavement under different explosion equivalents and buried depth. Tang[20] simulated the response of the pipeline under the condition of a large explosion and analyzed the dangerous sections and dangerous points of the pipeline underground explosion. Guo[21] proposed a numerical simulation method based on trinitrotoluene (TNT) equivalent, analyzed the impact failure law of shock wave on parallel pipelines, and proposed the safe spacing of natural gas parallel pipelines. Zhang[22] simulated the dynamic process of the underground pipeline after a ground explosion and studied the influence of internal pressure, TNT size, wall thickness, and buried depth on pipeline stress and strain. Zhang[23] defined the material parameters of a methane−air mixed gas cloud in ANSYS/LS-DYNA software and carried out the numerical calculation and experimental verification to prove its applicability.

Compared with the CFD method, the empirical model is simpler and takes less time and cost. Brode,[24] Baker,[25] Mills,[26] and Henrych[27] et al. proposed the general and equivalent fitting laws that correlate the maximum peak overpressure and shock wave attenuation with the explosive charge distance. According to the proportional distance, the peak overpressure of vapor cloud explosion can be predicted. Based on a large number of experimental verification and numerical simulation data, The Netherlands Organization[28] (TNO) obtained a set of explosive strength curves. According to different explosion intensities, the peak overpressure and normal phase duration of vapor cloud explosion can be obtained by reading the figure, which provides a theoretical basis for the proposal of a series of risk assessment methods.[29−32]

In summary, there are many methods to study the explosion problem, and most of the methods to study the explosion of solid explosives have been relatively mature. The method based on the equivalent assumption between combustible gas and TNT is also widely used in the study of vapor cloud explosion. However, it should be pointed out that there are essential differences between vapor cloud explosion and TNT explosion, which are mainly reflected in the following aspects.[33] The first aspect is reflected in the form of explosives. TNT belongs to condensed (liquid or solid) explosives, and methane gas cloud that reaches the explosion limit belongs to gas explosives. In addition to the different forms of explosives, TNT is much higher than methane gas cloud in density, detonation velocity, and detonation pressure, so the explosion power of the two is quite different. The second aspect is reflected in the size of the explosive source. The volume of the explosive source increases in the process of methane gas cloud explosion, but the volume of the explosive source is always ignored in TNT explosion. The last one is reflected in the detonation wave propagation velocity. The TNT explosion belongs to the detonation process, and the detonation wave propagation velocity decreases rapidly with the increase in detonation wave intensity. The explosion of methane gas cloud belongs to the detonation or in the transition process from detonation to detonation. The duration of positive detonation pressure is relatively short, and the duration of negative pressure is long.

In this paper, several widely used and representative empirical models and CFD methods are selected for comparative analysis, as shown in Table 1. The applicability of these methods in solving the problem of vapor cloud explosion is studied, which provides a theoretical basis for the further study of overpressure propagation under different building layouts.

Table 1. Several Widely Used and Representative Empirical Models and CFD Methods

	based on equivalent TNT assumption	others
empirical model	Henrych model, Mills model	TNO multi-energy method
CFD methods	the equivalent TNT method	the mixed gas method

https://doi.org/10.1021/acsomega.1c05332
ACS Omega 2021, 6, 34003−34020

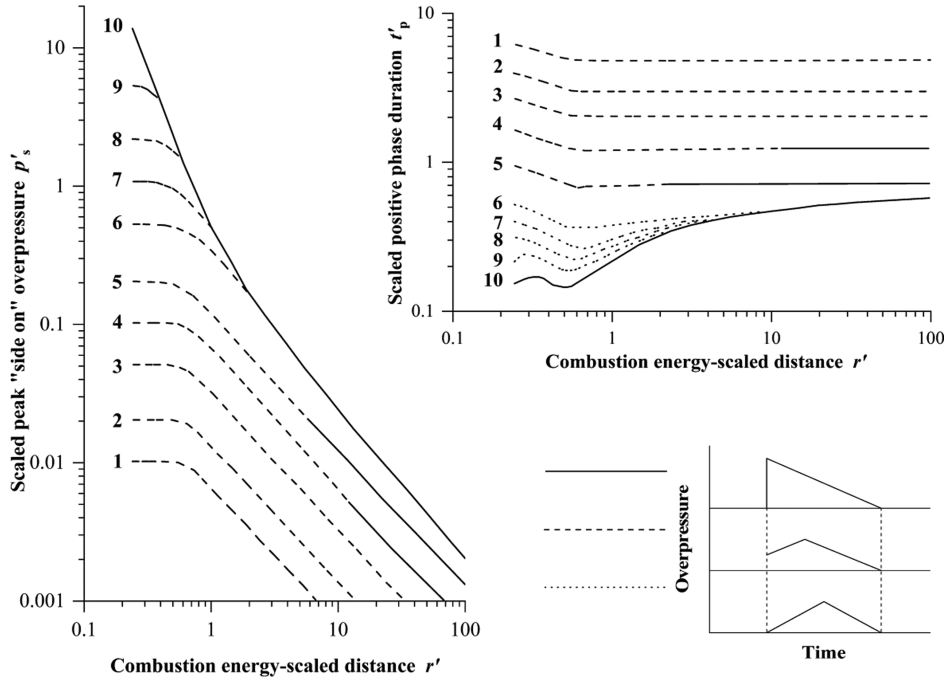

Figure 1. Parameter diagram of the TNO multi-energy method.

2.1.1. Method of Empirical Formula. The Henrych[27] model and Mills[26] model are based on the assumption of equivalence between the flammable material and TNT. The equivalent mass W_{TNT} can be calculated using eq 1 based on the total heat of combustion of flammable material.

$$W_{TNT} = \frac{\alpha \cdot W_f \cdot Q_f}{Q_{TNT}} \tag{1}$$

where α is an empirical explosion efficiency (2−15% for gas deflagration), W_f is the mass of flammable material, Q_f is the heat of combustion of flammable material, Q_{TNT} is the combustion of TNT, and W_{TNT} is the weight of TNT.

The premise of overpressure prediction of the vapor cloud explosion using the Henrych model and Mills model is to determine the scaled distance Z. The scaled distance Z is given as eq 2 using $W_{TNT}^{1/3}$.

$$Z = \frac{R}{W_{TNT}^{1/3}} \tag{2}$$

where R is the distance from the central point of the vapor cloud.

Henrych proposed one of the most common laws for blast wave attenuation in the free field of natural gas explosion, which is expressed as eq 3.

$$\Delta P_m|_{Henrych} = \begin{cases} \dfrac{14.072}{Z} + \dfrac{5.540}{Z^2} - \dfrac{0.357}{Z^3} + \dfrac{0.00625}{Z^4} & \text{if } 0.05 \le Z \le 0.3 \\ \dfrac{6.194}{Z} - \dfrac{0.326}{Z^2} + \dfrac{2.132}{Z^3} & \text{if } 0.3 \le Z \le 1 \\ \dfrac{0.662}{Z} + \dfrac{4.050}{Z^2} + \dfrac{3.288}{Z^3} & \text{if } 1 \le Z \end{cases} \tag{3}$$

Combined with the similarity theory and simulation model method, Mills proposed to simplify the well-known free field decay laws for gas explosion by modifying the evaluation distance. The corrected TNT explosion blast wave overpressure−distance decay relationship can be expressed as eq 4.

$$\Delta P_m|_{Mills} = \frac{0.108}{Z} - \frac{0.114}{z^2} + \frac{1.772}{z^3} \tag{4}$$

The TNO multi-energy method[28] is a typical scaled explosion prediction model. This method assumes that the vapor cloud is hemispherical and centrally ignited. Based on a large number of experimental verification and numerical simulation data, a set of explosion intensity curves (Figure 1) are obtained. In the application of the multi-energy method, it is necessary to select the appropriate explosion intensity level. The intensity level of the explosion source is any integer between 1 and 10, representing different explosion intensities. After determining the explosion intensity level, according to the scaled distance r', the scaled peak overpressure p'_s and the scaled duration time t'_p can be obtained from the characteristic curves of the explosion wave to calculate the overpressure and duration time of the explosion wave. The calculation method of each explosion parameter is as eqs 5−7

$$r' = r\left(\frac{E}{p_a}\right)^{-1/3} \tag{5}$$

$$p_s = p'_s p_a \tag{6}$$

$$t_p = t'_p \left(\frac{E}{p_a}\right)^{1/3} a_a^{-1} \tag{7}$$

2.1.2. Method of Numerical Simulation. ANSYS/LS-DYNA is a full-featured geometric nonlinearity (large displacement, large rotation, and large strain), material nonlinearity, and contact nonlinearity program. It is based on the Lagrange algorithm and has both Arbitrary Lagrangian Euler (ALE) and Euler algorithms. It has many element types, rich material

https://doi.org/10.1021/acsomega.1c05332
ACS Omega 2021, 6, 34003−34020

models, comprehensive contact analysis, load, initial conditions, and restraint functions. It is very suitable for solving nonlinear dynamic analysis and fluid−structure coupling problems of solid structures such as impact penetration, high-speed collision, and metal forming. It is widely used in aerospace, transportation, parts manufacturing, petroleum engineering, and other fields, and its calculation reliability has been proved by countless experiments.[34]

ANSYS/LS-DYNA can effectively predict the overpressure of the explosion shock wave. Similar to the Henrych and Mills models, the equivalent TNT method is also based on the assumption of equivalence between the flammable material and TNT. First, the explosion energy of the natural gas cloud is converted into equivalent TNT through eq 1. Second, the specific working conditions are modeled and meshed in ANSYS/LS-DYNA software. Compared with the unstructured grid (tetrahedron/pentahedron), the structured grid (hexahedron) is easier to be divided, and the accuracy is relatively high.[35] The finite element models established in this work adopt SOLID164 8 node hexahedral solid element. Third, the corresponding material parameters, constraints, and boundary conditions are set according to the engineering practice, and the ALE algorithm is combined to realize the coupling of the flow field and the solid field. Finally, the overpressure propagation law or the damage of explosion overpressure to the target object are obtained by calculation. The mixed gas method is similar to the equivalent TNT method, but the difference between the two methods is that the equivalent TNT method converts the energy of the vapor cloud explosion into equivalent TNT through the explosion empirical coefficient, and its essence is a solid-phase explosion, while the mixed gas method defines the material parameters of the methane−air mixed gas, whose essence is a gas-phase explosion.

2.2. Method Comparison and Verification. *2.2.1. Calculation of the Verification Example.* To verify the accuracy of equivalent TNT numerical simulation method, mixed gas numerical simulation method, Mills model, Henrych model, and TNO multi-energy method, these five methods are used to predict the overpressure of the full-scale explosion experiment of the gas pipeline carried out in ref 36, and the results are compared with the experimental data.

In the experiment, the volume of natural gas is 8×10^4 m^3, and the radius of the natural gas cloud is about 73 m according to the most dangerous concentration of 9.5%, which can be equiv to 24,575 kg TNT. The TNT explosive (dimension: 2.5 m × 2.5 m × 2.5 m) and hemispheric natural gas cloud (radius: 73 m) are established in ANSYS/LS-DYNA software. The MAT_HIGH_EXPLOSIVE_BURN constitutive model is used for both TNT and air−methane mixed gas. The EOS_JWL equation of state is used for TNT, and the EOS_LINEAR_POLYNOMIAL equation of state is used for air−methane mixed gas. The air material adopts the MAT_NULL constitutive model, and the equation of state is EOS_LINEAR_POLYNOMIAL. The parameter settings of each material and its equation of state are shown in Tables 2−4.[23,37,38]

Since the model is a symmetric model, to save computing time and avoid the calculation error caused by the excessive grid, only a 1/4 model is established for simulation calculation, and the influence on the results can be ignored.[39] The symmetry plane adopts normal constraint, and the fluid outer boundary adopts the non-reflecting boundary. The model grid adopts proportional division, and the grids near the TNT and mixed gas cloud are dense. With the increase in the distance from the explosion source, the grid size gradually increases. Both numerical simulation methods adopt the ALE algorithm to overcome the numerical calculation difficulty caused by the serious distortion of the element, to realize the dynamic analysis of the FSI. The monitoring points are set at the horizontal spacings of 100, 150, 200, 250, 300, and 400 m with the explosion source center, and the peak overpressure of each monitoring point under the two simulation methods is recorded. The physical model, constraint setting, boundary condition setting, and monitoring point location setting of the two numerical simulation methods are shown in Figure 2. The overpressure−time history curves of each monitoring point are shown in Figure 3.

Table 2. Parameters Setting of TNT Material and State Equation

initial density (kg/m^3)	detonation velocity (m/s)		detonation pressure (GPa)	A (GPa)	B (GPa)
1630	6930		27	371	3.231
$R1$	$R2$	ω	E_0 (MJ/m^3)		V_0
4.15	0.95	0.3	4290		1.0

Table 3. Parameter Settings of Methane−Air Mixture (9.5%) Material and State Equation

initial density (kg/m^3)	detonation velocity (m/s)		detonation pressure (MPa)	C_0 (Pa)	C_1	C_2
1.234	1855		1.87	0	0	0
C_3	C_4	C_5	C_6	E_0 (MJ/m^3)		V_0
0	0.274	0.274	0	3.408		1.0

Henrych model, Mills model, and TNO multi-energy method are used to predict the explosion overpressure of each monitoring point. In the application of the TNO multi-energy method, combined with the experimental conditions in ref 36 and the selection basis of the explosive intensity level (Table 5),[40] the explosive intensity level is determined as 7, 8, and 9. The peak overpressures of each monitoring point predicted by the abovementioned five methods are shown in Table 6.

2.2.2. Accurate Comparison of Methods. By comparing the predicted values obtained by the five methods with the experimental data (Figure 4), it can be seen that the predicted values of the Henrych model and Mills model are in good agreement, but in the near field, the overpressure prediction results of Mills model seem to be higher. Although the predicted values of the equivalent TNT method are higher than those of the Henrych model and Mills model, the variation trend of peak overpressure values of the three methods seems to be consistent. Compared with the experimental data, the calculated values of the three methods seriously underestimate the experimental results. In the near field of the explosion, the experimental data are about five times the predicted value. This may be due to the essential differences between the vapor cloud explosion and TNT explosion in the size change of the explosion source, the energy released at the moment of the explosion source, and the propagation velocity of the explosion shock wave. Therefore, the empirical model and numerical simulation based on the assumption of equivalence between the flammable material and TNT are not suitable for predicting the shock wave overpressure of natural gas deflagration.

Compared with the empirical model and numerical simulation methods based on the assumption of equivalence between the flammable material and TNT, it is found that the peak overpressure predicted by the TNO multi-energy method

https://doi.org/10.1021/acsomega.1c05332
ACS Omega 2021, 6, 34003−34020

Table 4. Parameter Settings of Air Material and State Equation

ρ (kg/m^3)	C_0 (Pa)	C_1	C_2	C_3	C_4	C_5	C_6	E_0 (MJ/m^3)	V_0
1.29	-1.0×10^5	0	0	0	0.4	0.4	0	0.25	1.0

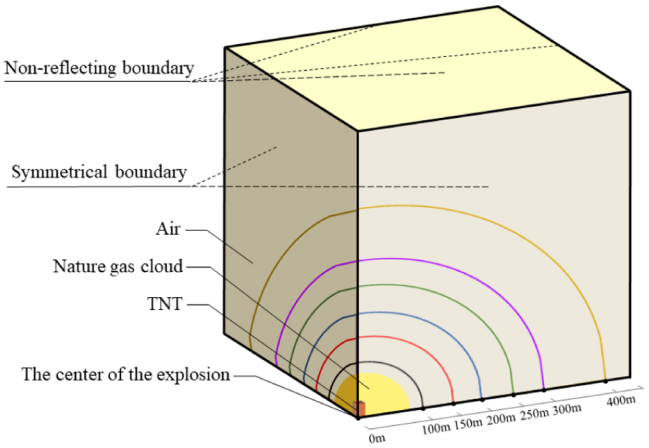

Figure 2. Physical model, constraint setting, boundary setting, and monitoring point position details of the two numerical simulation methods.

(level 8) and the mixed gas method is closer to the experimental data. However, the predicted value of the TNO multi-energy method in the near field underestimates the experimental data, and with the increase in distance, the predicted value overestimates the experimental data.

Overall, the mixed gas method is more suitable for exploring the overpressure problem of the vapor cloud explosion. The relative error between the predicted value and the experimental data at 100, 200, and 300 m is 12.93, 77.05, and 26.92%, respectively. Although the error at 200 m of the monitoring point with the sudden change in peak overpressure is larger, the error at the other monitoring points is less than 30%. Because the predicted values of all monitoring points are larger than the experimental data, the actual engineering safety design based on this method will not cause excessive casualties and property losses due to insufficient design margin. Therefore, this paper is based on the mixed gas method.

Table 5. Selection Basis of the Explosion Intensity Level

explosion intensity level	description
1	open space area
2	open space and few trees
3	open space, turbulence at first
4−7	some limited space
8−10	for process equipment

3. NUMERICAL SIMULATION

To explore the influence of different building layouts on the overpressure propagation of vapor cloud explosion, an investigation is carried out in a population-intensive high-consequence area of the gas pipeline. Four typical building layouts are summarized, as shown in Figure 5. Scenario 1: the vapor cloud explosion shock wave impacts a building vertically, scenario 2: the vapor cloud explosion shock wave passes through the gap between two horizontal layout buildings, scenario 3: the vapor cloud explosion shock wave impacts the building at a 45° angle, and scenario 4: the vapor cloud explosion shock wave passes through the gap between two vertical layout buildings.

Buildings can enhance or weaken the propagation of vapor cloud explosion overpressure. In the event of an accident, the premise of whether the building has a protective effect on people is that the building does not appear semi-overturn or completely overturn. According to the damage criterion of overpressure on people and buildings,[41] overpressure greater than 0.075 MPa can lead to the death of people, and overpressure greater than 0.076 MPa can lead to the collapse of buildings, considering 0.075 MPa as the extreme overpressure state of buildings and personnel and exploring the safety state of the building when the overpressure reaches 0.075 MPa and the influence of different building layouts on the overpressure propagation of the vapor cloud explosion.

3.1. Calculation of the Leakage Rate. After a buried gas pipeline leaks, natural gas will first diffuse into the soil. When the leak appears at the upper side of the pipeline, due to the pressure difference, it will cause a large upper and lower diffusion range,

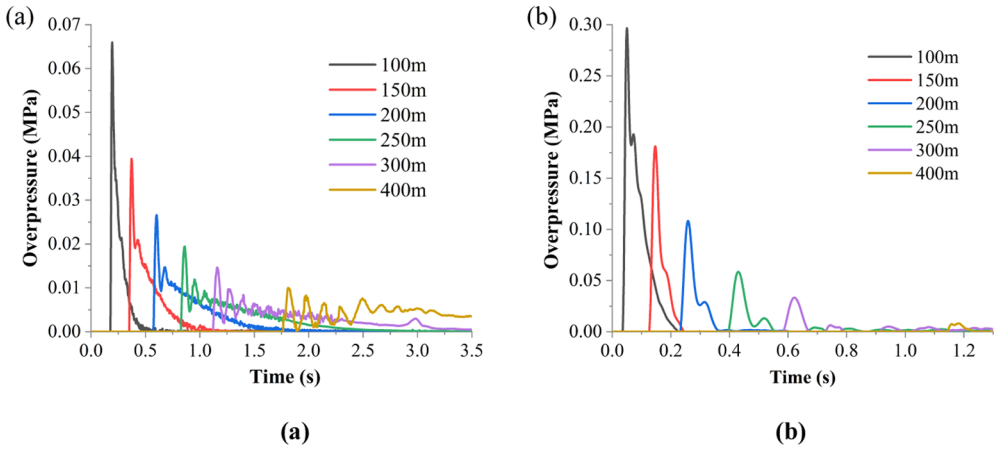

Figure 3. Overpressure time−history curves of each monitoring point by two numerical simulation methods. (a) Equivalent TNT method and (b) mixed gas parameter method.

https://doi.org/10.1021/acsomega.1c05332
ACS Omega 2021, 6, 34003−34020

Table 6. Peak Overpressure of Monitoring Points Predicted by Five Methods

distance from explosion point (m)	experimental data (MPa)	equivalent TNT method (MPa)	mixed gas method (MPa)	Henrych model (MPa)	Mills model (MPa)	TNO (level 7) (MPa)	TNO (level 8) (MPa)	TNO (level 9) (MPa)
100	0.2630	0.0660	0.2966	0.0523	0.0616	0.1115	0.2128	0.5066
150	0.0940	0.0394	0.1810	0.0268	0.0282	0.1013	0.2027	0.3040
200	0.0613	0.0266	0.1082	0.0173	0.0180	0.0811	0.1317	0.1317
250	0.0491	0.0194	0.0584	0.0125	0.0133	0.0648	0.0851	0.0851
300	0.0259	0.0147	0.0333	0.0097	0.0107	0.0557	0.0638	0.0638
400	0.0187	0.0100	0.0089	0.0079	0.0089	0.0314	0.0314	0.0314

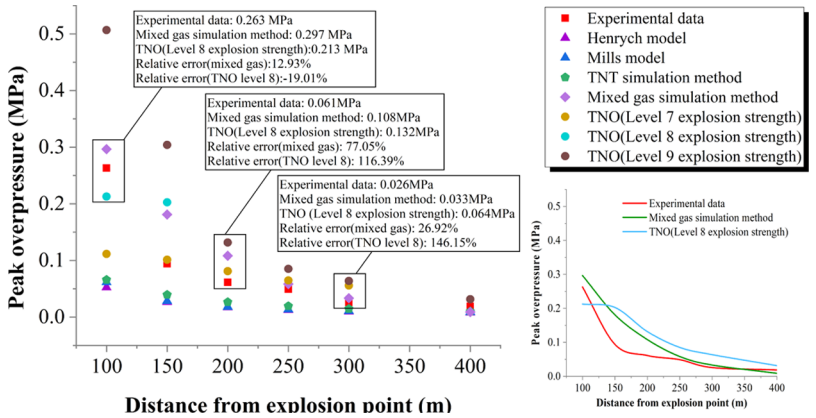

Figure 4. Comparison of predicted values from five methods with experimental data.

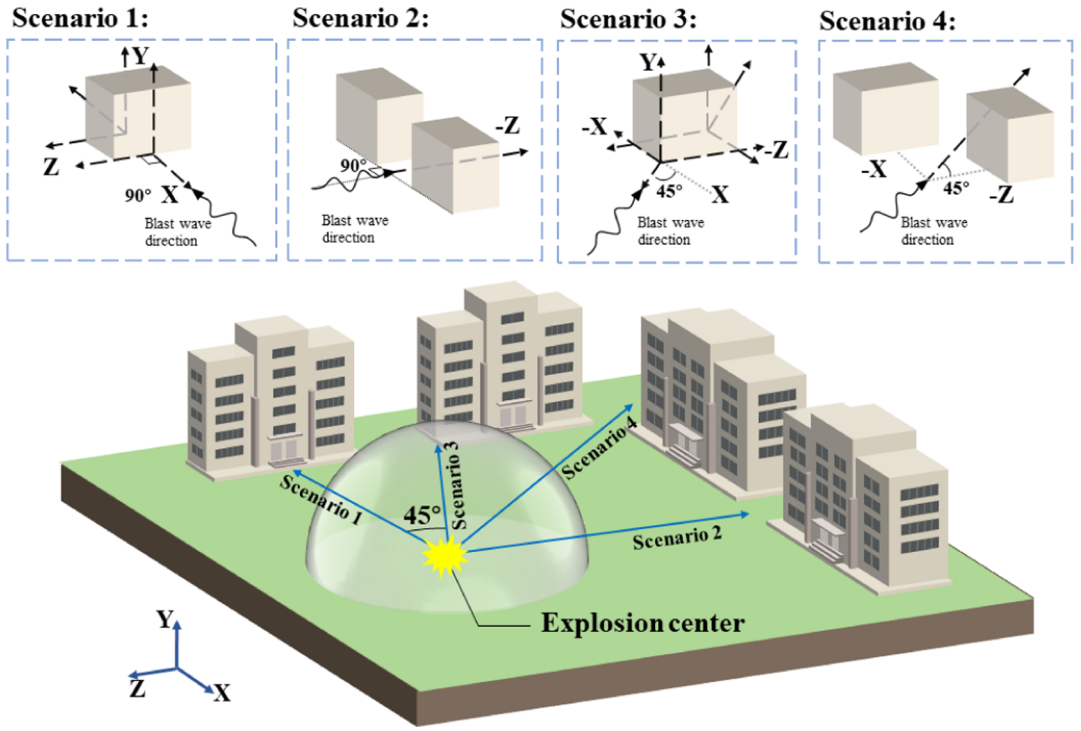

Figure 5. Layout diagrams of four typical buildings.

and a small left and right diffusion range, approximately an ellipsoid. However, as the diffusion range increases, this difference gradually weakens, and it is approximately spherical. Therefore, isotropy is assumed in the calculation, and the diffusion range of the leakage orifice is approximately equivalent to a sphere. The soil medium is usually a three-phase medium with pores in it. At the beginning of the leakage process, because the soil has a certain porosity, these pores will store some natural gas, so the actual nature gas cloud on the ground is not the total amount of the leakage. Therefore, the actual leakage of natural gas can be calculated using eqs 8−10.[42] The total leakage of natural gas can be calculated using eq 8.

$$Q_A = \alpha_0 c_0 A p_0 \cdot \sqrt{\frac{2 g_c M}{R_g T_0} \frac{\gamma}{\gamma - 1} \left[\left(\frac{p}{\rho_0} \right)^{2/\gamma} - \left(\frac{p}{\rho_0} \right)^{r+1/\gamma} \right]} \quad (8)$$

https://doi.org/10.1021/acsomega.1c05332
ACS Omega 2021, 6, 34003−34020

Table 7. Blast Parameters of Methane−Air Mixed Gas Explosion

methane concentration (%)	initial density (kg/m^3)	ratio of specific heat	detonation temperature (K)	detonation velocity (m/s)	detonation pressure (MPa)	instantaneous detonation pressure (MPa)	detonation heat (kJ/kg)	initial internal energy (kJ/m^3)
9.5	1.234	1.274	2815	1855	1.87	0.935	2762	3408
11.6	1.170	1.290	2450	1760	1.56	0.78	1890	2510

where Q_A is the total leakage of natural gas, α_0 is the viscosity coefficient (0.75−0.85 for buried pipeline and 0.61 for a sharp leak hole), A is the leakage orifice area, p_0 is the ambient atmospheric pressure, g_c is the gravitational constant, M is the molecular weight of the leaked gas, R_g is the ideal gas constant, γ is the adiabatic coefficient, and ρ_0 and T_0 are the density and temperature of the gas in the pipeline, respectively.

After the pipeline leaks, the part of natural gas absorbed by the soil can be calculated using eq 9.

$$Q_s = \int_0^r \frac{Q\varphi}{4\pi D_m r}\left(1 - \mathrm{erf}\left(\frac{r}{2\sqrt{D_m t}}\right)\right) \times 4\pi r^2 \mathrm{d}r_0 \quad (9)$$

where Q_s is the amount of natural gas leakage absorbed by the soil, φ is the soil porosity, D_m is the effective diffusion coefficient in the soil, r is the diffusion radius, erf is the error function, and t is the leakage time.

The mass of natural gas diffused into the air can be calculated using eq 10.

$$m = Q_A - Q_s \quad (10)$$

When the concentration of methane in the methane−air mixed gas is within the explosion limit (5−15%), the vapor cloud explosion will occur under certain ignition energy. Reference 23 gives the explosion parameters of the methane−air mixture when the methane concentration is 9.5 and 11.6%, respectively. As shown in Table 7, it can be seen that when the methane concentration is 9.5%, the explosion velocity and the explosion pressure are the largest.

According to the most dangerous volume fraction of natural gas cloud 9.5%, the volume of the natural gas cloud under different leakage time is calculated using eq 11.

$$r = \sqrt[3]{\frac{3m}{2\rho\pi\gamma}} \quad (11)$$

where r is the radius of natural gas cloud, m is the mass of natural gas leaked to the ground, ρ is the density of methane, and γ is the volume fraction of methane in the natural gas cloud.

The corresponding gas cloud volume are calculated when the leakage time is 1 and 2 h, as shown in Table 8.

Table 8. Natural Gas Leakage and Corresponding Natural Gas Cloud Radius at Different Leakage Time

leak time (h)	Q_A(kg)	Q_s (kg)	m (kg)	natural gas cloud radius (9.5%) (m)
1	772.07	318.48	453.59	14
2	1519.9	626.96	892.94	18

3.2. Establishment of the Numerical Model. *3.2.1. Finite Element Model for State Verification of Building Structure under Extreme Overpressure.* The multi-story building is simplified into a frame structure consisting of columns, beams, and floor slabs. Column size is 45 × 45 cm, floor thickness is 15 cm, and each layer height is 300 cm, with a total of five layers. The unit system adopts cm−g−μs, and the SOLID164 hexahedral element in LS-DYNA is selected to mesh the building model. The air grid size is 50 cm, and the building grid size is 15 cm. The plane layout of the building structure, and the finite element model for state verification of the building structure under extreme overpressure is shown in Figure 6.

3.2.2. Finite Element Model of Influence of Different Building Layouts on Overpressure Propagation. Since the influence of buildings on overpressure propagation is only explored, the building is simplified as a block with a size of 1485 × 2445 × 1500 cm, and the material is reinforced concrete. The SOLID164 hexahedral element in LS-DYNA is selected to mesh the air and building models, and the mesh size is 50 cm. The finite element models of influence of the different building layouts on overpressure propagation are shown in Figure 7.

3.3. Fluid-Structure Interaction Theory. The FSI aims to study the structure in the fluid field that is displaced and deformed due to the action of the fluid. Conversely, the displacement and deformation of the structure will also change the pressure and velocity distribution of the flow field. The changes in the flow field will further deform the structure, thereby forming a continuous coupling between the fluid and the structure. Using the FSI to realize the interaction between the explosion shock wave, the building can make the calculation result closer to the actual situation.

Generally speaking, Lagrange formulations are often used in computational solid mechanics, and Euler formulations are used in computational fluid mechanics. However, when solving the FSI problems, an algorithm that combines the two methods is required, namely, arbitrary Lagrange−Euler (ALE) algorithm. The ALE algorithm combines the advantages of the Lagrange method and the Euler method, and the computational grid can move independently of the material configuration and the spatial configuration. In this way, the mobile interface of the object can be accurately described by specifying the appropriate mesh motion form, and the element can maintain a reasonable shape during the movement, avoiding the defects of pure Lagrange description and pure Euler description. This can overcome the numerical calculation difficulties caused by the severe distortion of the element and realize the dynamic analysis of the FSI.

3.4. Material Constitutive Model and Parameters. *3.4.1. Constitutive Model of Air Material.* The air material model selects the air material MAT_NULL and the fluid dynamic material linear polynomial equation EOS_LINEAR_-POLYNOMIAL.[35] Its state equation form is

$$P = C_0 + C_1\mu + C_2\mu^2 + C_3\mu^3 + (C_4 + C_5\mu + C_6\mu^2)\rho_0 E \quad (12)$$

where ρ_0 is the initial density of the gas, E is the initial internal energy per unit volume, V is the relative volume, and C_i is the constant (i=0−6).

This equation can be changed to γ state equation for the ideal gas, where $C_0 = C_1 = C_2 = C_3 = C_6 = 0$ and $C_4 = C_5 = \gamma - 1$, that is, the air is simplified as a non-viscous ideal gas, and the equation of state is transformed into

https://doi.org/10.1021/acsomega.1c05332
ACS Omega 2021, 6, 34003−34020

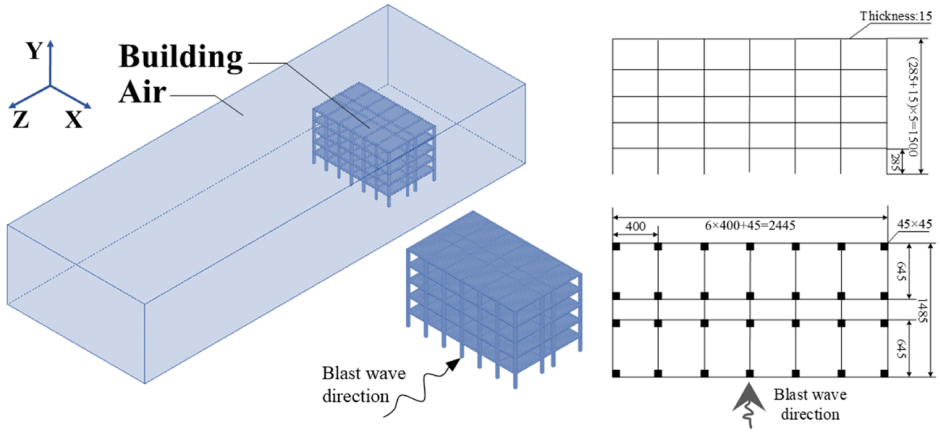

Figure 6. Finite element model for state verification of the building structure under extreme overpressure.

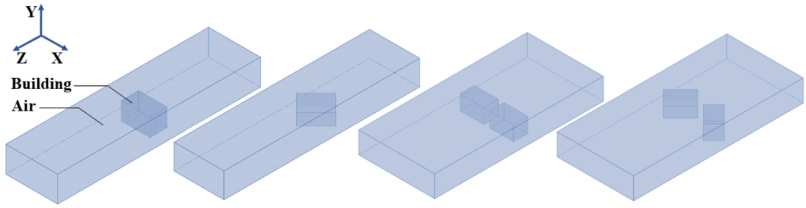

Figure 7. Finite element models of influence of the different building layouts on overpressure propagation.

Table 9. Parameter Settings of the Concrete Material

density (kg/m^3)	Young's modulus (GPa)	Poisson's ratio	tensile limit (MPa)	shear limit (MPa)	compressive yield stress (MPa)	shear retention
2500	30	0.2	2.5	14.5	28.97	0.03

$$P = (\gamma - 1)\frac{\rho}{\rho_0}E_0 \tag{13}$$

where γ is ideal gas isentropic adiabatic index (1.4), and ρ_0 is the gas density.

The material parameters and equation of state for air are shown in Table 3.

3.4.2. Constitutive Model of the Methane–Air Mixture Gas Material. Methane–air mixture adopts an * MAT _ HIGH _ EXPLOSIVE _ BURN constitutive model and EOS _ LINEAR _ POLYNOMIAL equation of state. INITIAL _ VOLUME _ FRACTION _ GEOMETRY is used to fill the hemispherical methane–air mixture in the air domain, and INITIAL _ DETONATION is used to control the fire source position. The parameter settings of the methane–air mixture (9.5%) material and state equation are shown in Table 2.

3.4.3. Constitutive Model of the Concrete Material. The MAT _ BRITTLE _ DAMAGE[35] constitutive model is adopted for the reinforced concrete material, which is proposed by Govindjee, Kay, and Simo. It is an anisotropic brittle damage model to simulate the dynamic response of concrete under tension and compression, the shear failure, and the high strain rate. The material model considers that the elastic stiffness of the material will be reduced by the occurrence of microcracks under tension, thereby reducing the shear strength and elastic strength of the material. Once a point in the structure reaches the critical tensile strength, there will be tiny cracks at this point, and its vertical direction is the same as the first principal stress direction. Once a crack occurs, it will be fixed in the position where it just appears and changes with the change in the element position. The elastic strength perpendicular to the plane direction of the crack will automatically decrease. It is realized by softening the elastic modulus of the crack surface, that is, to keep the crack surface consistent with the constraints expressed in the following formula

$$\sigma - f_n + (1 - \varepsilon)f_n(1 - e^{-H\alpha}) \leq 0 \tag{14}$$

where f_n is the initial principal tensile strength of the material, ε is the small constant; H is the softening modulus, α is an internal variable, and σ is the calculated stress.

The parameter settings of the concrete and steel bar are shown in Tables 9 and 10.[43]

Table 10. Parameter Settings of the Steel bar

fraction of reinforcement in section(%)	Young's modulus (GPa)	yield stress (MPa)	hardening modulus (GPa)	failure strain
0.8	200	335	1.18	0.1

For brittle materials such as stone, cast iron, concrete, and glass, most cases are in the form of fracture failure, and the first strength theory and the second strength theory can be adopted. For plastic materials such as copper and carbon steel, they usually fail in the form of yield, and the third strength theory and the fourth strength theory can be adopted. In the process of the building structure being impacted by vapor cloud explosion, the building structure usually cracks and shatters. In the process of finite element numerical simulation, the breaking and shattering of materials can be achieved by deleting the element. A threshold is set for the material in advance. When calculating, software will test the stress and strain of each element, and the unit that

https://doi.org/10.1021/acsomega.1c05332
ACS Omega 2021, 6, 34003−34020

reaches the threshold will be deleted, realizing the failure of the material. Accurate control of material failure is directly related to the accuracy of numerical simulation results.

Because the compressive property of the concrete material is much higher than its tensile property, there will be a large number of concrete elements that fail due to the tensile stress reaching the tensile limit of the material in the process of explosion shock. Therefore, the failure control of the concrete material needs to be considered from the two failure states of tension and compression. The compressive strength of the concrete element is controlled by the parameters of the material constitutive model itself, and the failure of the concrete element under tensile stress is controlled by parameters in the additional control card. Because the MAT _ BRITTLE _ DAMAGE constitutive model itself does not have failure control, the MAT _ ADD _ EROSION keyword is used to control the failure of concrete materials. The tensile strength and compressive strength of concrete are 2.01 and 20.1 MPa, respectively. The steel material can be approximately regarded as an isotropic homogeneous material, so the failure control of the steel material only needs to control its strain. The failure strain is set in the material constitutive model, and the value is 0.1.

3.5. Setting of Boundary Conditions and Restrains. Explosion waves propagate in infinite air. Treating the boundary conditions with fixed boundary nodes will cause reflection and refraction of blast waves at the boundary, which will lead to mutual overlap between blast waves. As a result, significant errors will occur in the solution process. At present, the best way to solve this problem is to use non-reflecting boundary conditions, which are based on the principle that when finite field conditions are applied to solve infinite field problems, dampers are artificially added to the finite boundary conditions of the model. In this way, the energy of the blast wave will not propagate and decay in a single finite field. Instead, it generates a projection of the wave as it passes through the boundary. Thus, the problem is still treated as an infinite field problem. Such a method not only ensures the accuracy of the computational model but also saves time significantly.[22]

Therefore, the non-reflecting boundary condition is applied to the outer boundary of the fluid grid. In terms of constraints, the bottom of the building structure is fixed, and the normal displacement constraint is applied on the symmetrical surface of the model.

4. RESULTS AND DISCUSSION

4.1. Overpressure Propagation of the Vapor Cloud Explosion under the Condition of No Building Occlusion. The overpressure caused by the vapor cloud explosion under the condition of no building occlusion is predicted, and the peak overpressure distributions of the vapor cloud explosions at 1 and 2 h of pipeline leakage are obtained. Combined with the damage criterion of overpressure to personnel, the damage ranges of overpressure of the vapor cloud explosion under different leakage time are shown in Table 11, and the overpressure−time history curves are shown in Figure 8. The peak overpressure of different monitoring points at 1 and 2 h of pipeline leakage is fitted, and the peak overpressure−distance curves of the vapor cloud explosion are obtained, as shown in Figure 9.

4.2. State of the Building Structure under Extreme Overpressure. According to the distribution of peak overpressure under the condition of no building occlusion (Table 11), the overpressure of the vapor cloud explosion generated by pipeline leakage for 1 h reaches 0.075 MPa at 45 m from the explosion center. The vapor cloud explosion overpressure generated by pipeline leakage for 2 h reaches 0.075 MPa at 57 m from the explosion center.

Table 11. Overpressure Injury Level and Range for Humans

overpressure (MPa)	injury level	impact range (m)	
		leakage for 1 h	leakage for 2 h
>0.075	fatal	<45	<57
0.045−0.075	serious	45−52	57−71
0.025−0.045	moderate	52−62	71−81
0.01−0.025	slight	62−80	81−96
<0.01	safe	>80	>96

Figure 10 shows the damage of the building structure under extreme overpressure. It can be found that the top layer near the explosion source has obvious deformation, and there are A, B, and C three damages. The first damage occurred at A, followed by the simultaneous damage at B and C on both sides of A. The damage at B and C is smaller than that at A. With the increase in leakage time, the damage degree of A, B, and C gradually increases, and there are also damages at D, E, and F, but the damage degree is smaller than that of A, B, and C. Only the floor is damaged, while the column does not appear to be damaged. Overall, the building structure does not show semi-overturn or overturning phenomenon, in a safe state.

4.3. Overpressure Propagation of the Vapor Cloud Explosion under the Condition of Different Building Layouts. *4.3.1. Scenario 1.* The explosion center is located on the extension line of the middle line of the building. The vapor cloud explosion shock wave impacts the building vertically, setting up monitoring points along with three directions from the midpoint on both sides of the building, respectively. The distance between the monitoring points is 1.5 m, and each direction has 15 monitoring points. The monitoring points are set, as shown in Figure 5.

Figures 11 and 12 show the peak overpressure distributions in three directions on both sides of the building when the vapor cloud explosion shock wave formed at 1 and 2 h of pipeline leakage vertically impacts the building, respectively.

The peak overpressure distributions in three directions in the front side of the building are analyzed. It can be seen from Figure 11a that the peak overpressure of the vapor cloud explosion increases significantly at the position near the front edge of the building. The peak overpressure increases from 0.075 to 0.138 MPa and 0.153 MPa at 1 and 2 h of pipeline leakage, respectively, by about 84 and 104%. With the decrease in the distance from the explosion source, compared with the peak overpressure under the condition of no building occlusion, the peak overpressure under the condition of building occlusion increases first and then decreases and finally tends to be consistent. From Figures 11b,c, we can see that with the increase in height and the offset to both sides of the middle line of the building, the peak overpressure gradually decreases. In the first half of the curves, the peak overpressure under the condition of building occlusion is completely higher than that under the condition of no building occlusion, while in the latter halves, it shows the opposite situation. This is because the reflection and superposition of the explosion shock wave occur in the area blocked by the building, which increases the peak overpressure sharply, while the peak overpressure in the area without being blocked decreases, even lower than the peak overpressure under the condition of no building occlusion.

https://doi.org/10.1021/acsomega.1c05332
ACS Omega 2021, 6, 34003−34020

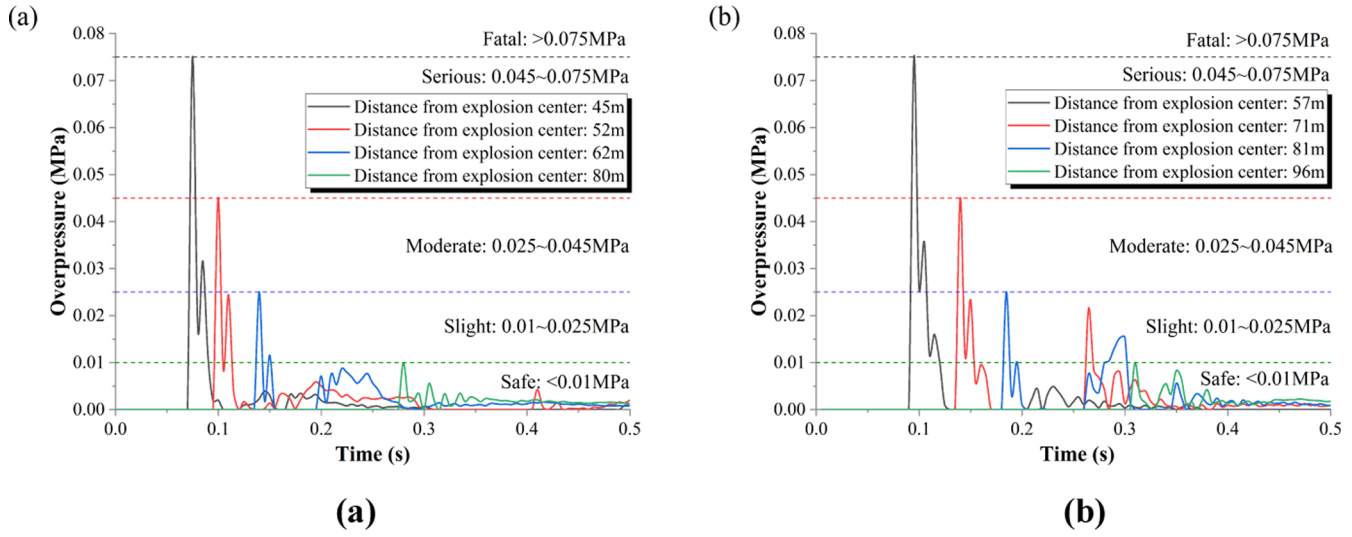

Figure 8. Overpressure−time history curves of the boundary of the injury level range with leakage time of 1 and 2 h. (a) Leakage for 1 h and (b) leakage for 2 h.

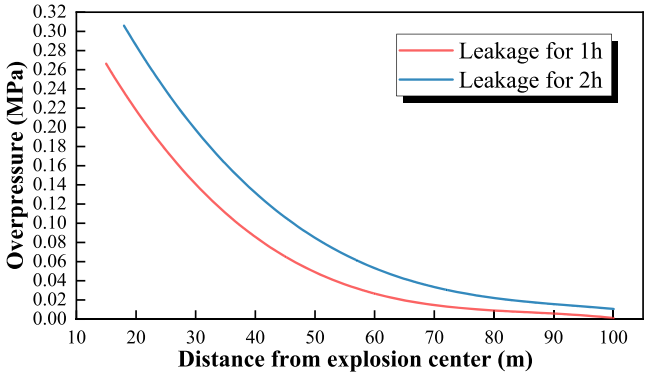

Figure 9. Overpressure−distance fitting curves with leakage time of 1 and 2 h.

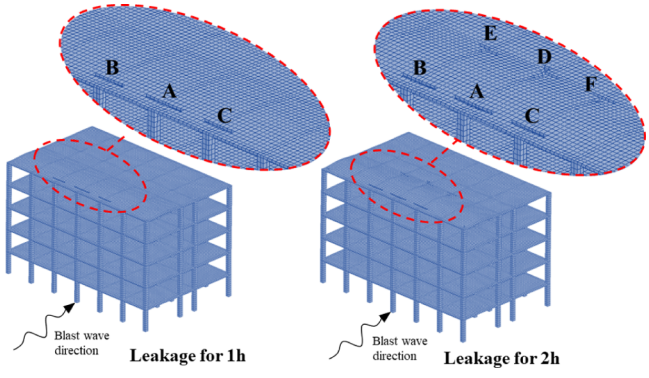

Figure 10. Damage condition of the building structure under ultimate overpressure.

The peak overpressure in the area blocked by the building is mostly above 0.075 MPa. According to the damage criterion of overpressure on personnel, it is the "Fatal" area. In the area not blocked by the building, the peak overpressure is below 0.075 MPa, and the lowest is 0.007 MPa. Although it does not cause death, it cannot be ignored.

The peak overpressure distributions in three directions in the backside of the building are analyzed. It can be seen from Figure 12a that the peak overpressure behind the building has a significant decrease. At the position close to the rear edge of the building, the peak overpressure decreases from 0.034 to 0.004 MPa at 1 h of pipeline leakage and decreases from 0.038 to 0.005 MPa at 2 h of pipeline leakage, respectively, by 88 and 87%. Peak overpressure overall change is not big, but there is a large rise at 7 m behind the building. The shock wavefront expands in a hemispherical shape around the open space. When the shock wave front contacts the building, the shock wave on the front side of the building is blocked by the building, reflecting, superimposing, and converging, resulting in an increase in peak overpressure. At this time, the shock wavefront, which is not blocked by the building, is split by the building and continues to expand forward. It meets again at 7 m behind the building and reflects and superimposes, resulting in the peak overpressure rising again. However, since the building largely weakens the propagation of overpressure, the peak overpressure is still smaller than that without building occlusion. From Figure 12b,c, we can see that with the increase in height and the offset to both sides of the middle line of the building, the peak overpressure gradually decreases. The peak overpressure of the obscured area by the building decreases, while the peak overpressure increases in the area not obscured. However, the overall peak overpressure is less than that under the condition of no building occlusion, which is contrary to the changes in overpressure in the front side of the building. Buildings have blocking and shielding effects on the overpressure of the explosion side and non-explosion side, respectively. The blocking effect causes the overpressure to rise, while the shielding effect causes the overpressure to decrease. Therefore, the differences on both sides of the building also lead to the opposite trend of peak overpressure changes on both sides of the building.

The peak overpressure in the area obscured by the building is mostly below 0.01 MPa. According to the damage criterion of overpressure to personnel, it is the "Safe" area. For the area not obscured by the building, the peak overpressure is between 0.01 and 0.025 MPa, which is the "Slight" area.

The peak overpressure is compared with and without building occlusion, and the correction factor σ is defined. The peak overpressure P_0 at a certain distance without building occlusion can be obtained from Figure 9, and the correction factor σ can be obtained from Figure 13. The peak overpressure of the vapor

https://doi.org/10.1021/acsomega.1c05332
ACS Omega 2021, 6, 34003−34020

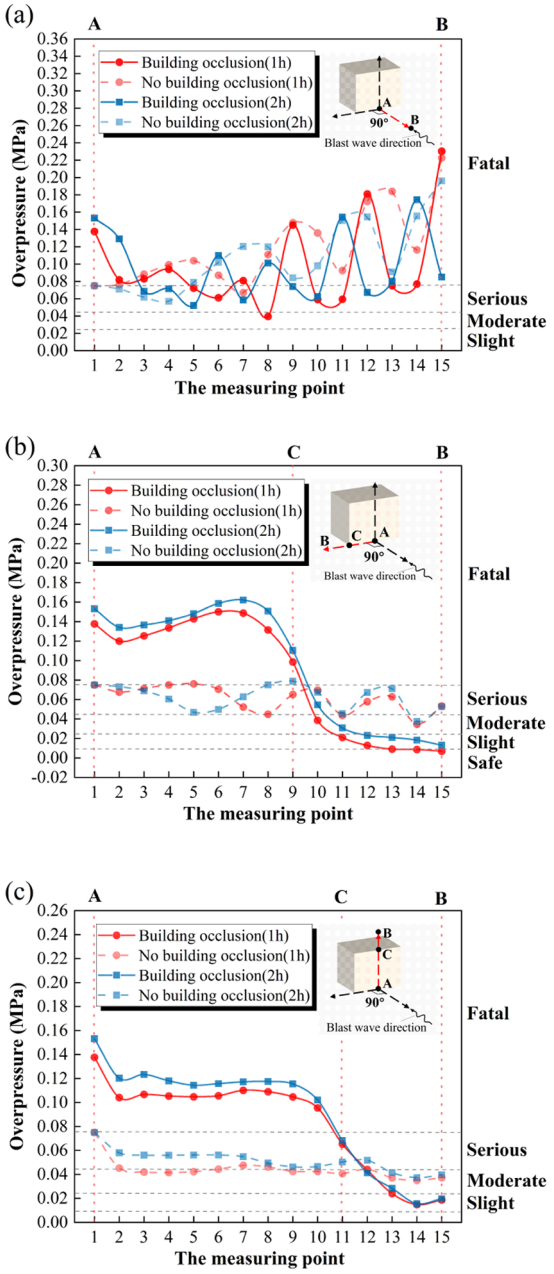

Figure 11. Peak overpressure distribution in three directions in front of the building. (a) Direction: gradually approaching the explosion source from the building; (b) direction: gradually shifting from the middle line of the building to one side; and (c) direction: gradually shifting upward from the ground.

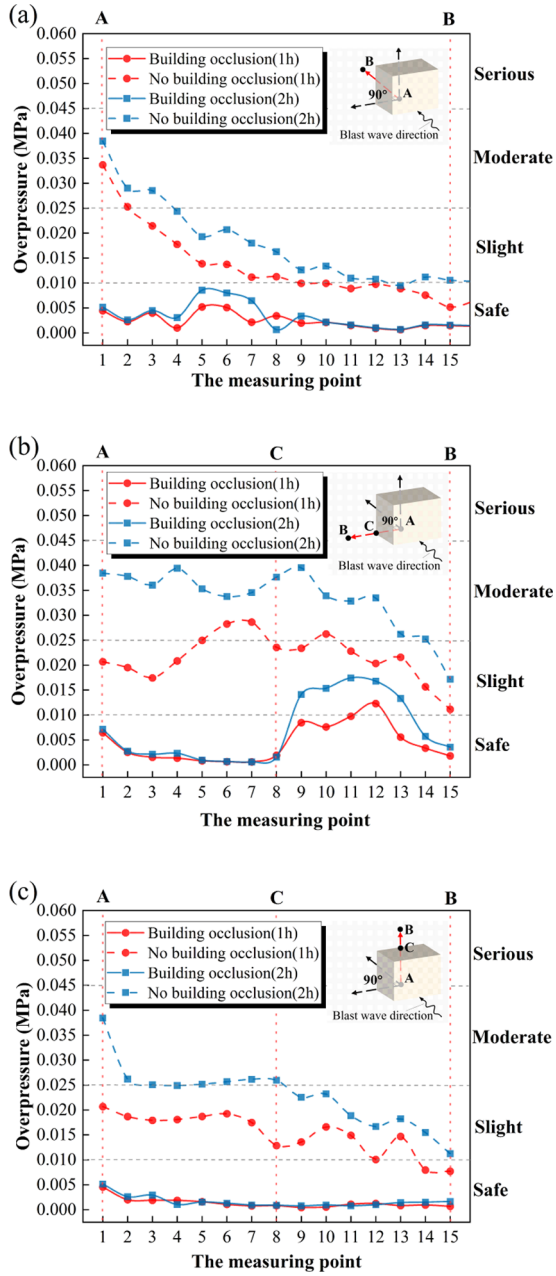

Figure 12. Peak overpressure distribution in three directions behind the building. (a) Direction: gradually away from the explosion source from the building; (b) direction: gradually shifting from the middle line of the building to one side; and (c) direction: gradually shifting upward from the ground.

cloud explosion blocked or obscured by buildings can be roughly calculated using eq 15.

$$P = \sigma P_0 \tag{15}$$

It can be seen from Figure 13 that in the front side of the building near the front edge of the building, $\sigma > 1$, indicating that the building has an enhanced effect on overpressure. However, as the distance from the explosion source decreases, the σ value fluctuates below 1 axis, $\sigma < 1$, which is less than the peak overpressure under the condition of no building occlusion, and eventually tends to be consistent, $\sigma = 1$. On the backside of the building, the σ value is completely less than 1. Overall, the multi-story building has a significant influence on the overpressure propagation of the vapor cloud explosion. The building has a blocking and shielding effect on the overpressure propagation on both sides of the building, which increases the overpressure on the front side and decreases the overpressure on the backside. With the increase in leakage time, the enhancing effect of overpressure is more obvious, and the weakening effect is weaker.

4.3.2. Scenario 2. The explosion center is located on the extension line of the middle line A, B of the gap between the two horizontal layout buildings. The vapor cloud explosion shock wave passes through the gap. According to GB 5018-93 "Urban residential area planning and design specifications," the distance between the two buildings is set to 6 m. Taking the point A as the

https://doi.org/10.1021/acsomega.1c05332
ACS Omega 2021, 6, 34003−34020

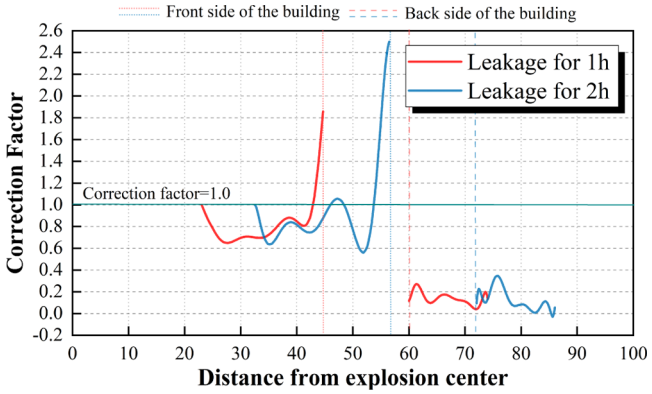

Figure 13. Diagram of the peak overpressure correction factor on both sides of a building when the explosive shock wave impacts the building vertically.

starting point, 18 monitoring points are set backward, and the distance between the monitoring points is 1.5 m. The monitoring points are set, as shown in Figure 5.

Figure 14 shows the peak overpressure distributions of the middle line A, B of the gap when the vapor cloud explosion shock wave formed at 1 and 2 h of pipeline leakage passes through the gap.

It can be seen from Figure 14 that after the shock wavefront passes through the A point between two horizontal layout buildings, it is blocked by the building. At this time, the reflection and superposition degree of the shock wave is low, resulting in the overall peak overpressure being lower than that without building occlusion and fluctuating greatly. However, in the latter half of the gap A, B, with the movement of the shock wavefront in the building gap, the reflection and superposition of the shock wave become higher, and the peak overpressure exceeds the peak overpressure without building occlusion. When the pipeline leakage time is 1 and 2 h, the peak overpressure at the maximum increase in peak overpressure increases from 0.035 to 0.046 MPa, from 0.037 to 0.059 MPa, which increases by about 29.5 and 56.5%, respectively. This may be caused by the reflection and refraction of the shock wave when it touches the building. After point B, due to the impact wavefront has passed through the building gap, the overpressure is greatly weakened by the building, and the peak overpressure decreases overall compared with the case without building occlusion.

On the whole, with the increase in leakage time, the peak overpressure increases. When the leakage time is 1 and 2 h, the peak overpressure of the gap between the two horizontal layout buildings is basically above 0.045 MPa. According to the damage criterion of overpressure on personnel, it belongs to the "Moderate" and "Serious" areas.

4.3.3. Scenario 3. The explosion center is located on the extension line of the angle dividing line of the two exterior walls (near the explosion source) of the building. The vapor cloud explosion shock wave impacts the building at an angle of 45°. The intersection points of the external walls (near and far from the explosion source) of the building are taken as their starting points, and the monitoring points are set in four directions. The distance between the monitoring points is 1.44 m. There are 18 monitoring points for the long wall, 11 monitoring points for the short wall, 10 monitoring points for the building near the explosion source direction, and 15 monitoring points for the other directions. The monitoring points are set, as shown in Figure 5.

Figures 15 shows the peak overpressure distributions of the four directions near the explosion source when the vapor cloud explosion shock wave formed by 1 and 2 h of pipeline leakage impacts the building at an angle of 45°.

The peak overpressure distributions in four directions near the explosion source are analyzed. It can be seen from Figure 15a that the peak overpressure of the vapor cloud explosion increases significantly at the position near the front edge of the building. The peak overpressure increases from 0.075 to 0.101 MPa and 0.112 MPa at 1 and 2 h of pipeline leakage, respectively, by about 35 and 49%. As the decrease in the distance from the explosion source, the peak overpressure decreases relatively until it conforms to the trend of peak overpressure under the condition of no building occlusion. It can be seen from Figure 15b that with the increase in height, the peak overpressure gradually decreases. In the first half of the curves, because the shock wavefront is blocked by the building when it contacts the building, the shock wave is reflected, superimposed, and converged, increasing the peak overpressure. Therefore, the peak overpressure with building occlusion is completely higher than that without building occlusion. In the latter part of the curves, the height of the measuring point exceeds the height of the building, and the impact wavefront is not blocked by the building. Therefore, the peak overpressure with building occlusion is lower than that without building occlusion. The overall trend of the peak overpressure is consistent with that in scenario 1 (the vapor cloud explosion shock wave impacts a

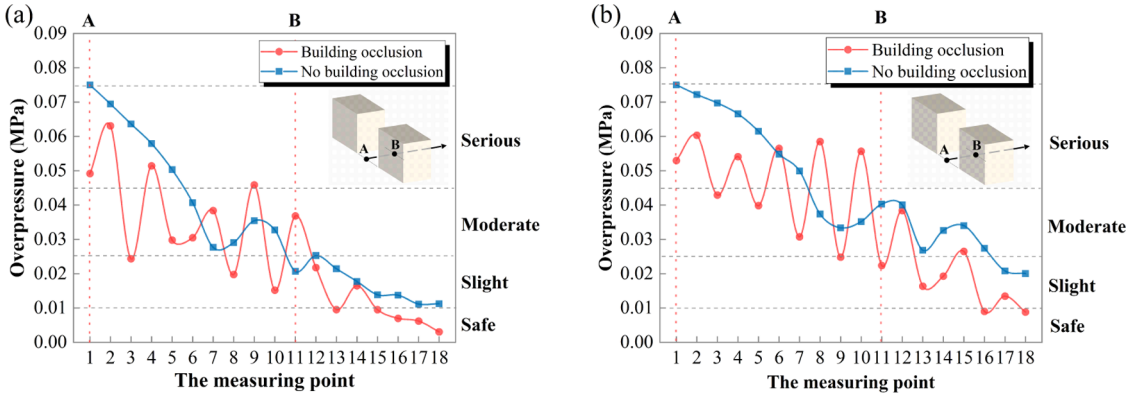

Figure 14. Peak overpressure distribution of the gap between two horizontal layout buildings. (a) Leakage for 1 h. (b) Leakage for 2 h.

https://doi.org/10.1021/acsomega.1c05332
ACS Omega 2021, 6, 34003−34020

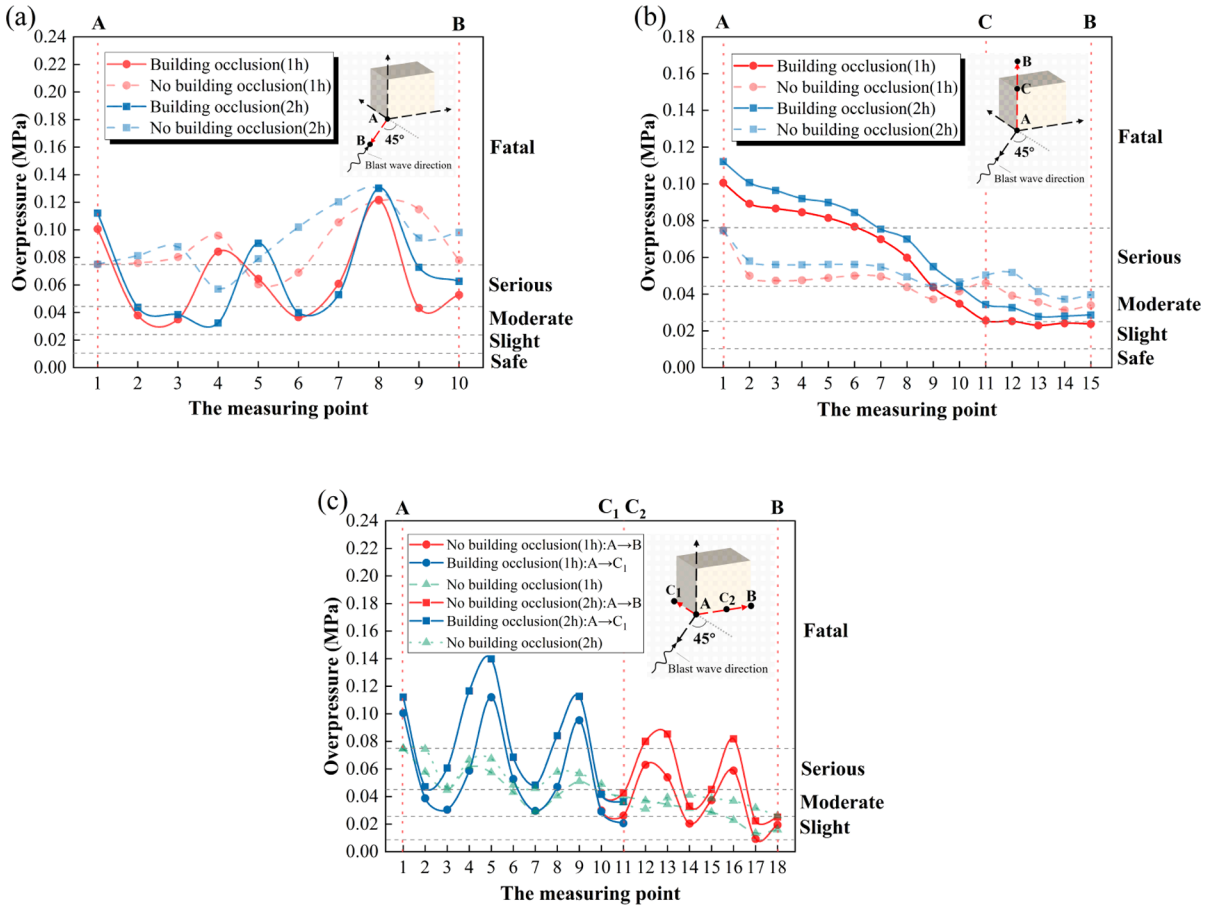

Figure 15. Peak overpressure distribution of the four directions in the front of the building. (a) Direction: gradually approaching the explosion source from the building; (b) direction: gradually shifting upward from the ground; and (c) direction: starting from the intersection of two walls and gradually moving away from the explosion source along the wall.

building vertically), and the difference is that scenario 1 has a significantly greater effect on the increase in overpressure. It can be seen from Figure 15c that the maximum overpressure enhancement is located at the edge of the building near the explosion source, rather than at point A. The peak overpressure increases from 0.057 to 0.112 MPa at 1 h of pipeline leakage and increases from 0.067 to 0.140 MPa at 2 h of pipeline leakage, respectively, by 95 and 107%. Because the building is not symmetrical about line AB, although the angle is the same, the length is different. The first half of the two peak overpressure curves are coincident, and the peak overpressure is higher than that under the condition of no building occlusion. However, near point C, due to the lack of building occlusion, the degree of shock wave reflection and superposition is low, resulting in the peak overpressure near the short wall being lower than that near the long wall.

The peak overpressure in the area blocked by the building is mostly above 0.075 MPa. According to the damage criterion of overpressure to personnel, it can cause death, belonging to the "Fatal" area. The peak overpressure of the area not blocked by the building is below 0.045 MPa, which will not cause death but may cause discomfort, belonging to the "Moderate" area.

The peak overpressure distributions in four directions behind the building are analyzed. It can be seen from Figure 16a that compared with the peak overpressure under the condition of no building occlusion, the peak overpressure at the backside of the building has a significant decrease, and the change fluctuates greatly, and the peak overpressure at some monitoring points even exceeds that without building occlusion. The peak overpressure near the building decreases the most. The peak overpressure decreases from 0.0096 to 0.0045 MPa at 1 h of pipeline leakage and increases from 0.0105 to 0.0051 MPa at 2 h of pipeline leakage, respectively, by 53 and 51%. It also has a reduction effect on overpressure, but the weakening effect is weak. As far away from the explosion source, the peak overpressure curves show several peaks, which is slightly different from scenario 1. It can be seen from Figure 16b that with the increase in height, the peak overpressure gradually decreases. The peak overpressure under the condition of building occlusion is completely lower than that without building occlusion. It is different from the peak overpressure change in scenario 1 (the vapor cloud explosion shock wave impacts a building vertically), possibly due to the fact that the blast wave has become weak where it arrives. As a result, the overall overpressure only shows a weakening trend. It can be seen from Figure 16c,d that with the increase in the distance from the explosion source, the peak overpressure near the building gradually decreases, and the change fluctuates greatly. The peak overpressure under the condition of building occlusion is much lower than that under the condition of no building occlusion. When the pipeline leaks for 1 h, the maximum reduction rates of peak overpressure near the long wall and the short wall are 93 and 85%, respectively. When the pipeline leaks for 2 h, the maximum reduction rates of overpressure near the long wall and the short wall are 88 and 82%, respectively.

https://doi.org/10.1021/acsomega.1c05332
ACS Omega 2021, 6, 34003−34020

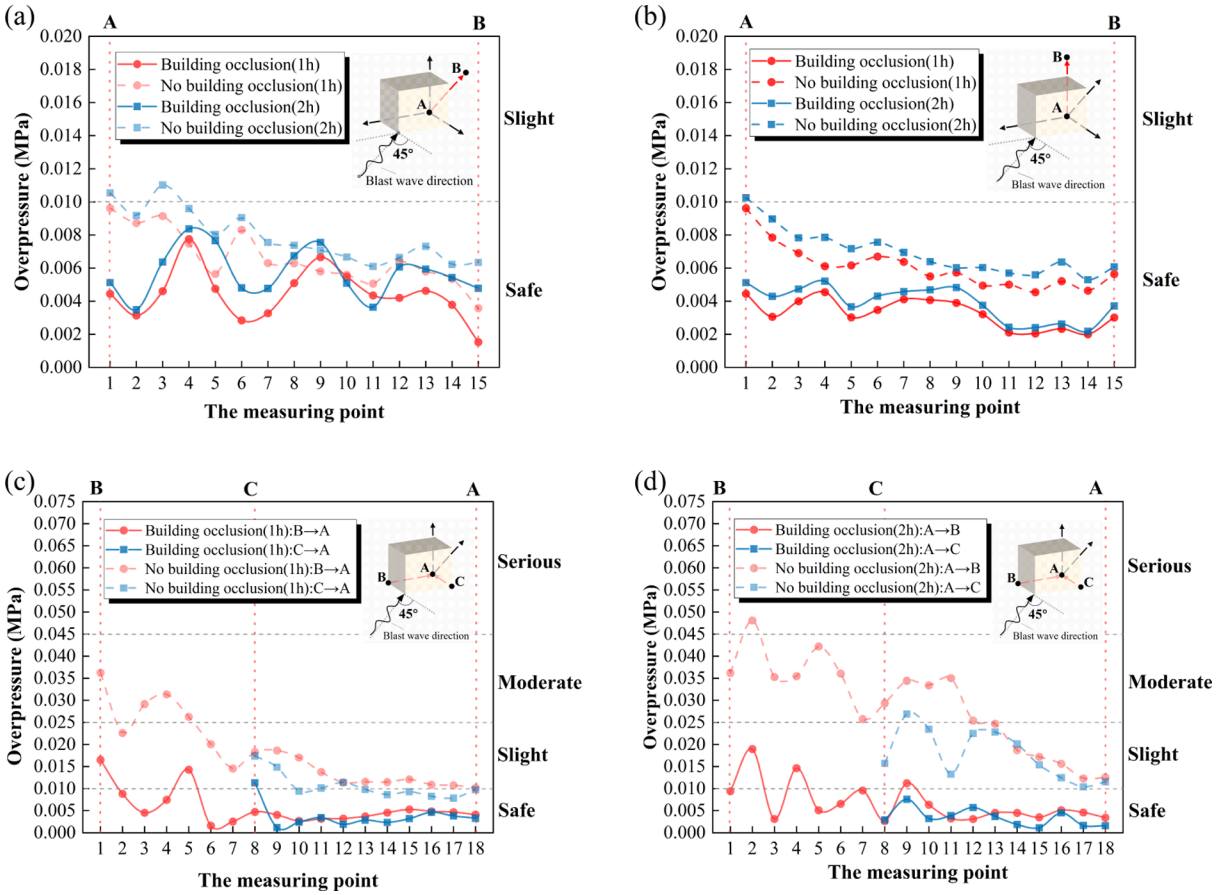

Figure 16. Peak overpressure distribution of the four directions behind the building. (a) Direction: gradually away from the explosion source from the building; (b) direction: gradually shifting upward from the ground; (c) direction: starting from the intersection of two walls and gradually moving away from the explosion source along the wall (leakage for 1 h); and (d) direction: starting from the intersection of two walls and gradually moving away from the explosion source along the wall (leakage for 2 h).

The peak overpressure in the area obscured by the building is mostly below 0.01 MPa. According to the damage criterion of overpressure to personnel, it is the "Safe" area.

The peak overpressure is compared with and without building occlusion, and the correction factor σ is defined. The peak overpressure P_0 at a certain distance without building occlusion can be obtained from Figure 9, and the correction factor σ can be obtained from Figure 17. The peak overpressure of the vapor cloud explosion blocked or obscured by buildings can be roughly calculated using eq 16.

$$P = \sigma P_0 \tag{16}$$

It can be seen from Figure 17 that in the front side of the building near the front edge of the building, $\sigma > 1$, indicating that the building has an enhanced effect on overpressure. However, as the distance from the explosion source decreases, the σ value fluctuates below 1 axis, $\sigma < 1$, which is less than the peak overpressure under the condition of no building occlusion, and eventually tends to be consistent, $\sigma = 1$. On the backside of the building, the σ value is completely less than 1.

In general, the influence law on overpressure is similar to that in scenario 1 (the vapor cloud explosion shock wave impacts a building vertically), but compared with scenario 1, scenario 3 (the vapor cloud explosion shock wave impacts a building at an angle of 45°) has a smaller effect on the enhancing of overpressure on the front side of the building and the weakening of overpressure on the backside of the building.

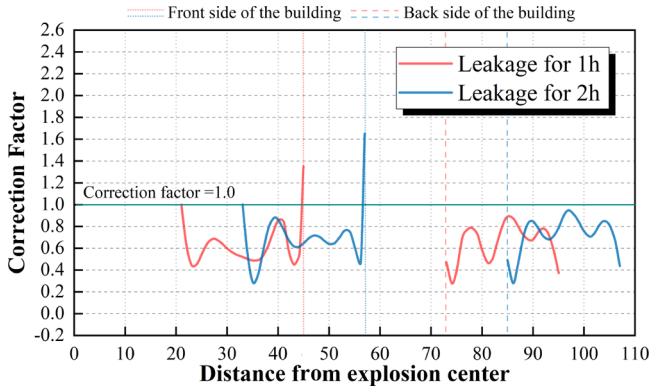

Figure 17. Diagram of the peak overpressure correction factor on both sides of a building when the explosive shock wave impacts the building at an angle of 45°.

4.2.1. Scenario 4. The explosion center is located on the extension line of the middle line A, B of the gap between the two vertical layout buildings. The distance between the two buildings is 6 m. Taking point A as the starting point, 18 monitoring points are set backward, and the distance between the monitoring points is 1.5 m. The monitoring points are set, as shown in Figure 5.

Figure 18 shows the peak overpressure distributions of the middle line A, B of the gap when the vapor cloud explosion

https://doi.org/10.1021/acsomega.1c05332
ACS Omega 2021, 6, 34003−34020

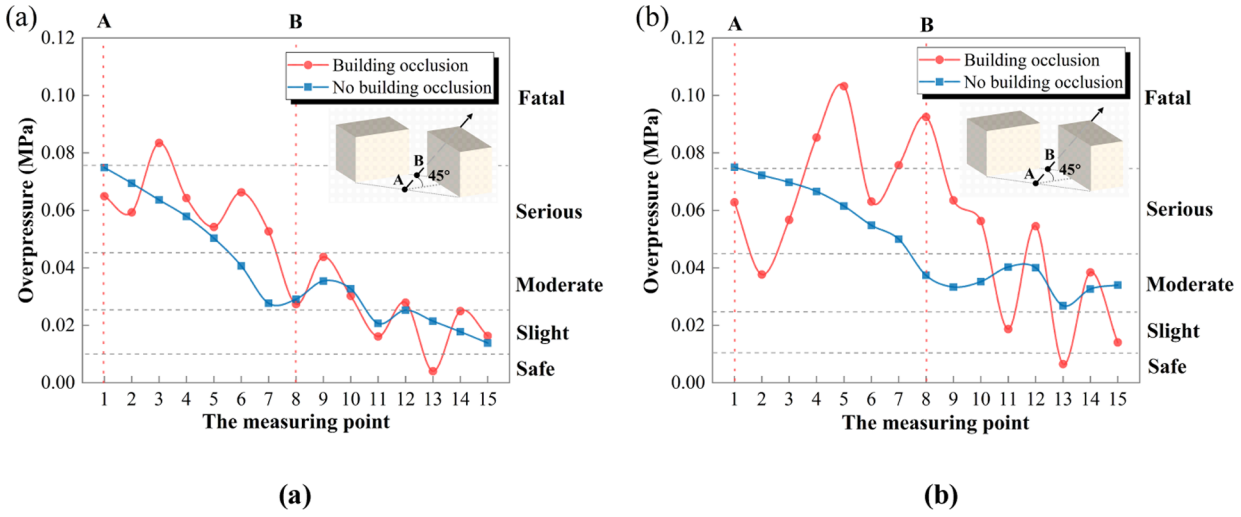

Figure 18. Peak overpressure distribution of the gap between two vertical layout buildings. (a) Leakage for 1 h and (b) leakage for 2 h.

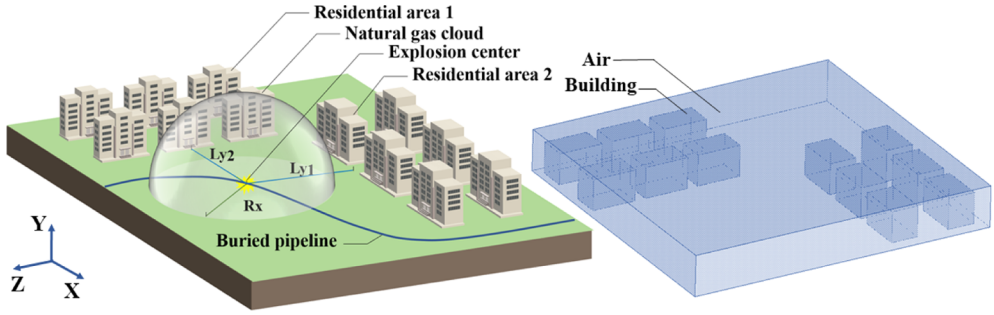

Figure 19. Schematic diagram of the actual scene and finite element model.

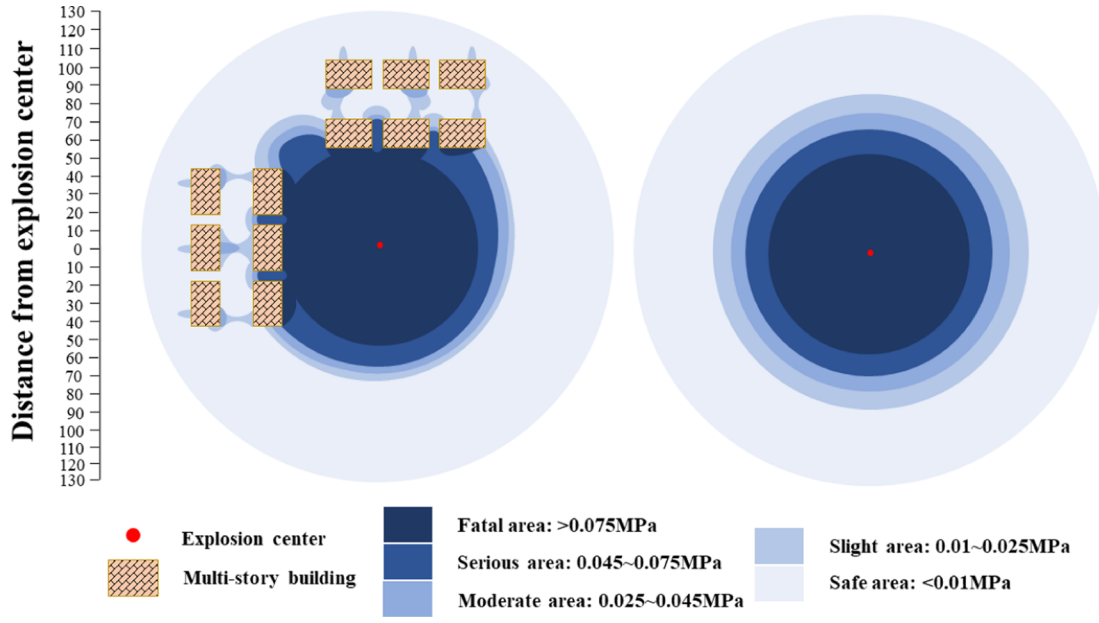

Figure 20. Damage level range of personnel with and without building occlusion.

shock wave formed at 1 and 2 h of pipeline leakage passes through the gap.

As can be seen from Figure 18, under the condition of building occlusion, the overpressure peak decreases first due to the low reflection and superposition degree of the shock wave after the shock wavefront passes through point A. However, with the decrease in the distance from the "poort" B, the reflection and superposition degree of the shock wave become higher due to the occlusion of the building, and the peak overpressure completely exceeds the peak overpressure under the condition of no building occlusion and fluctuates relatively large. The peak overpressure increases from 0.028 to 0.053 MPa at 1 h of

https://doi.org/10.1021/acsomega.1c05332
ACS Omega 2021, 6, 34003−34020

pipeline leakage and increases from 0.037 to 0.093 MPa at 2 h of pipeline leakage, respectively, by 90.3 and 147.46%. However, after "poort" B, the impact wavefront has passed through the building gap, weakened by the building, peak overpressure overall decline, fluctuating around the curve of the peak overpressure under the condition of no building occlusion. With the increase in leakage time, the peak overpressure increases as a whole. At the leakage time of 1 and 2 h, the peak overpressure of the A, B section between the two vertical layout buildings can reach more than 0.075 MPa, which belongs to the "Fatal" area. After B point, the peak overpressure is less than 0.075 MPa, although it will not cause death, it can still cause damage to personnel.

However, compared with scenario 2 (the vapor cloud explosion shock wave passes through the gap between two horizontal layout buildings), due to the "poort" formed by the two buildings, the reflection and superposition of shock waves are more obvious. The increase rates of the peak overpressure in the front of the "poort" in scenario 4 (the vapor cloud explosion shock wave passes through the gap between two vertical layout buildings) are bigger than that in scenario 2. The overpressure increase rates at the maximum increase at 1 and 2 h of leakage increased by 60 and 91%, respectively. After the "poort" B, compared with scenario 2, the peak overpressure and the fluctuation amplitude of change in scenario 2 are also larger.

5. EXAMPLE COMPUTATION

Taking a typical scenario of a population-intensive high-consequence area as an example, the pipeline is buried underground, and there are two residential areas along the pipeline. It is assumed that there is a small hole leakage in the pipeline, and the leakage time is 2 h. The natural gas leaks into the air and mixes with the air to form a natural gas cloud and explodes. To determine the damage range of the vapor cloud explosion overpressure under the influence of buildings, the finite element model is established in ANSYS/LS-DYNA software, and the peak overpressure distribution is determined. Combined with the damage criterion of overpressure on personnel, the safety level range of the scene is divided. The schematic diagram of the actual scene and finite element model is shown in Figure 19.

When the natural gas cloud explodes, combined with the calculated overpressure peak distribution and the damage criterion of overpressure to personnel, the safety grade ranges with and without building occlusion are plotted, as shown in Figure 20.

It can be seen from Figure 20 that under the explosion shock of the same explosion source, the damage level range with or without building occlusion is completely different. Under the condition of building occlusion, due to the explosion shock wavefront being a hemisphere to spread around, the damage level range presents a concentric circle, and the damage level decreases from the explosion source to the outside. However, the damage level range is no longer presented as a concentric circle under the condition of no building occlusion.

The damage level of the area on the explosion side of the building increased. The area on the explosion side of the buildings in the front row is elevated to the "Fatal" area, and that in the rear row is elevated to the "Moderate" area. In the gap formed by the buildings, the effect of the gap formed by the irregular layout of the buildings on the overpressure is significantly greater than that of the gap formed by the horizontal layout of the buildings, and the damage level is improved to some extent. The damage level decreased on the side of the building away from the explosion source. Therefore, the study on the influence of different building layouts on the vapor cloud explosion overpressure can provide a theoretical basis for the reasonable determination and optimization of safe evacuation routes.

6. CONCLUSIONS

In this work, several commonly used CFD methods and empirical models for overpressure prediction, such as Mills model, Henrych model, TNO multi-energy method, equivalent TNT method, and mixed gas method, were systematically compared and analyzed, and the optimal method for studying the overpressure problem of vapor cloud explosion was determined. The overpressure propagation law of vapor cloud explosion under different building layouts is studied, and the reference basis for the determination and optimization of the emergency evacuation path of personnel in the high-consequence areas of the gas pipelines is put forward. The conclusions are as follows:

(1) The CFD methods and empirical models based on the equivalent assumption between TNT and combustible gas are suitable for the study of solid-phase explosion but not for the study of gas-phase explosion. The comparison shows that the mixed gas method based on CFD is more suitable for exploring the overpressure problem of vapor cloud explosion. The predicted overpressure value is generally higher than the actual overpressure value, and the error is small. The safety design of pipeline engineering based on this method will fully consider the design margin to avoid the accidental casualties caused by insufficient design.

(2) The peak overpressure distribution of the vapor cloud explosion is completely different with or without building occlusion. In the case of direct occlusion of buildings, buildings have blocking and shielding effects on overpressure propagation on the explosion side and non-explosion side, which can enhance and weaken the overpressure, respectively. Different orientations of buildings have different effects on the enhancement and weakening of the overpressure. On the explosion side of the building, when the angle between the building and the shock wave direction is 90 and 45°, the maximum increase rate of overpressure is close, about 90%. The increase rate of overpressure on the non-explosion side of the building is also similar, about 90%, but at 90°, the enhancement and weakening of overpressure are more stable. The propagation of overpressure in the gap formed by the two buildings is also affected by the buildings. The gap of different structures formed by buildings with different orientations has different enhancement effects on overpressure. Due to the "poort" between the two vertical layout buildings, the blocking effect on overpressure is stronger, and the enhancement effect of overpressure is more obvious. The increase rate is more than 60% higher than the horizontal layout.

(3) Based on the analysis of the peak overpressure distribution of vapor cloud explosion, the following principles should be followed in the determination and optimization of the emergency evacuation path: (a) the non-explosion side of the building should be preferentially selected, and the weakening effect of the building on

https://doi.org/10.1021/acsomega.1c05332
ACS Omega 2021, 6, 34003−34020

overpressure should be used to reduce the damage of overpressure to personnel; (b) based on principle a, buildings with an angle of 90° to the blast wave are preferred, which have a stable weakening effect on overpressure; and (c) when it is necessary to pass through the building gap, the gap formed by two horizontally arranged buildings should be given priority. Following the above principles to determine and optimize the safe evacuation path can minimize the damage of explosion overpressure to personnel.

In summary, this study determined the optimal method selection of vapor cloud explosion overpressure and provided suggestions for the subsequent study of vapor cloud explosion overpressure. The overpressure propagation law of vapor cloud explosion under different building layouts is studied, which provides a theoretical basis for the safety design of gas pipelines and the safety control of high-consequence areas. However, this research also has insufficiency, only has studied the overpressure question, which is one of three big threats in the high-consequence area explosion, and has not studied the thermal radiation effect and the explosive fragment ejection, two big threats. Considering the influence of different building layouts on these three threats, it will provide a very important reference for determining the safe evacuation path and the safe distance of pipeline laying. This will be an important research direction in the field of safety evaluation of high-consequence areas of gas pipelines, which is of great significance.

AUTHOR INFORMATION

Corresponding Author

Hongye Jiang − *College of Petroleum & Gas Engineering, Southwest Petroleum University, Chengdu 610500, China; Oil & Gas Pipeline Technology Research Institute, Chengdu 610037, China*; Email: j822422@126.com

Authors

Minghua Chi − *College of Petroleum & Gas Engineering, Southwest Petroleum University, Chengdu 610500, China; Oil & Gas Pipeline Technology Research Institute, Chengdu 610037, China*; orcid.org/0000-0002-0430-0612

Xubin Lan − *College of Petroleum & Gas Engineering, Southwest Petroleum University, Chengdu 610500, China; Chengdu Branch of Sinopec Petroleum Engineering Design Co.,Ltd., Chengdu 610000, China*

Taolong Xu − *College of Petroleum & Gas Engineering, Southwest Petroleum University, Chengdu 610500, China; Oil & Gas Pipeline Technology Research Institute, Chengdu 610037, China*

Yi Jiang − *Southwest Pipeline Co., Ltd of China Oil & Gas Pipeline Network Corporation, Chengdu 610037, China*

Complete contact information is available at: https://pubs.acs.org/10.1021/acsomega.1c05332

Funding

The author(s) disclosed receipt of the following financial support for the research, authorship, and/or publication of this article. This research is supported by the Scientific and Technological Innovation Team for the Safety of Petroleum Tubular Goods in Southwest Petroleum University (grant number: 2018CXTD01) and Open Fund Project of Oil Gas Fire Protection Key Laboratory of Sichuan Province (YQXF201601).

Notes

The authors declare no competing financial interest.

REFERENCES

(1) *China Natural Gas Development Report*; National Energy Administration, 2020.

(2) Zhang, S.; Feng, X.; Wang, X.; Feng, Q.; Han, Y. Status and whole process management system of high consequence areas of oil and gas pipelines in China. *Youqi Chuyun* **2021**, *40*, 521−526.

(3) Cui, Y.; Quddus, N.; Mashuga, C. V. Bayesian network and game theory risk assessment model for third-party damage to oil and gas pipelines. *Process Saf. Environ. Prot.* **2020**, *134*, 178−188.

(4) Qin, G.; Zhang, P.; Hou, X.; Wu, S.; Wang, Y. Risk assessment for oil leakage under the common threat of multiple natural hazards. *Environ. Sci. Pollut. Res.* **2020**, *27*, 16507−16520.

(5) Peng, W.; Zhang, J.; Yuan, H.; Fu, M. Numerical simulation on influence of leakage hole on gas leakage in deep buried pipeline. *Zhongguo Anquan Shengchan Kexue Jishu* **2020**, *16*, 59−64.

(6) Zhu, Y.; Qian, X.-m.; Liu, Z.-y.; Huang, P.; Yuan, M.-q. Analysis and assessment of the Qingdao crude oil vapor explosion accident: Lessons learnt. *J. Loss Prev. Process Ind.* **2015**, *33*, 289−303.

(7) Chi, M.; Jiang, H.; Zhao, X.; Xu, T. Analysis on leakage and explosion accidents in high consequence areas of gas pipeline based on UHBs. *Zhongguo Anquan Shengchan Kexue Jishu* **2021**, *17*, 41−47.

(8) Guo, Y.; Liu, C.; Wang, D.; He, R. Numerical study and safety spacing of buried parallel gas pipelines: a study based on TNT equivalent method. *Int. J. Pressure Vessels Piping* **2018**, *168*, 246−257.

(9) Xu, T.; Yao, A.; Zeng, X.; Li, Y. Study on the security conditions of parallel laying gas transmission pipelines under blast loading. In *ICPTT 2011: Sustainable Solutions For Water, Sewer, Gas, And Oil Pipelines*, 2011; pp 1401−1411.

(10) Meng, Q.; Wu, C.; Li, J.; Wu, P.; Xu, S.; Wang, Z. A study of pressure characteristics of methane explosion in a 20 m buried tunnel and influence on structural behaviour of concrete elements. *Eng. Failure Anal.* **2021**, *122*, 105273.

(11) Qian, H.; Zong, Z.; Wu, C.; Li, J.; Gan, L. Numerical study on the behavior of utility tunnel subjected to ground surface explosion. *Thin-Walled Structures* **2021**, *161*, 107422.

(12) Sevim, B.; Toy, A. T. Blasting Response of a Two-Storey RC Building Under Different Charge Weight of TNT Explosives. *Iran. J. Sci. Technol.* **2020**, *44*, 565−577.

(13) Sun, X.; Li, W.; Huang, Q.; Zhang, J.; Sun, C. Large eddy simulations of wind loads on an external floating-roof tank. *Engineering Applications of Computational Fluid Mechanics* **2020**, *14*, 422−435.

(14) Farzaneh-Gord, M.; Faramarzi, M.; Ahmadi, M. H.; Sadi, M.; Shamshirband, S.; Mosavi, A.; Chau, K.-w. Numerical simulation of pressure pulsation effects of a snubber in a CNG station for increasing measurement accuracy. *Engineering Applications of Computational Fluid Mechanics* **2019**, *13*, 642−663.

(15) Ghalandari, M.; Shamshirband, S.; Mosavi, A.; Chau, K.-w. Flutter speed estimation using presented differential quadrature method formulation. *Engineering Applications of Computational Fluid Mechanics* **2019**, *13*, 804−810.

(16) Mou, B.; He, B.-J.; Zhao, D.-X.; Chau, K.-w. Numerical simulation of the effects of building dimensional variation on wind pressure distribution. *Engineering Applications of Computational Fluid Mechanics* **2017**, *11*, 293−309.

(17) Chen, W.; Zhu, Z. Numerical simulation of wind turbulence by DSRFG and identification of the aerodynamic admittance of bridge decks. *Engineering Applications of Computational Fluid Mechanics* **2020**, *14*, 1515−1535.

(18) Salih, S. Q.; Aldlemy, M. S.; Rasani, M. R.; Ariffin, A. K.; Ya, T. M. Y. S. T.; Al-Ansari, N.; Yaseen, Z. M.; Chau, K.-W. Thin and sharp edges bodies-fluid interaction simulation using cut-cell immersed boundary method. *Engineering Applications of Computational Fluid Mechanics* **2019**, *13*, 860−877.

(19) Zhuohua, Y.; Qing, Y.; Zhenzhen, J.; He, L. Numerical Simulation of Pipeline-Pavement Damage Caused by Explosion of Leakage Gas in Buried PE Pipelines. *Adv. Civ. Eng.* **2020**, 1−18.

(20) Tang, Q.; Jiang, N.; Yao, Y.; Zhou, C.; Luo, X.; Wu, T. Safety assessment of buried gas pipeline subject to surface explosion: A case study in Wuhan, China. *Eng. Failure Anal.* **2021**, *120*, 105119.
(21) Guo, Y.; He, L.; Wang, D.; Liu, S. Numerical investigation of surface conduit parallel gas pipeline explosive based on the TNT equivalent weight method. *J. Loss Prev. Process Ind.* **2016**, *44*, 360−368.
(22) Zhang, L.; Liang, Z.; Zhang, J. Mechanical response of a buried pipeline to explosion loading. *Journal of Failure Analysis and Prevention* **2016**, *16*, 576−582.
(23) Zhang, X.; Wu, Y.; Li, Y. Numerical analysis of dynamic responses of steel frame structure subjected to internal gas explosion. *Engineering Mechanics* **2013**, *30*, 358366−359362.
(24) Brode, H. L. Blast wave from a spherical charge. *Phys. Fluids* **1959**, *2*, 217.
(25) Baker, W. E.; Cox, P. A.; Kulesz, J. J.; Strehlow, R. A.; Westine, P. S. *Explosion Hazards and Evaluation*; Elsevier Amsterdam, 1983.
(26) Mills, C. The design of concrete structures to resist explosions and weapon effects. *Int. Conf. Hazard Prot.* **1988**.
(27) Henrych, J.; Major, R. *The Dynamics of Explosion and its Use*; Elsevier Amsterdam, 1979.
(28) Mercx, W. P. M.; Van den Berg, A. C. The explosion blast prediction model in the revised CPR 14E(yellow book). *Process Saf. Prog.* **1997**, *16*, 152−159.
(29) Lv, D.; Tan, W.; Liu, L.; Zhu, G.; Peng, L. Research on maximum explosion overpressure in LNG storage tank areas. *J. Loss Prev. Process Ind.* **2017**, *49*, 162−170.
(30) Wesevich, J.; Hassig, P.; Nikodym, L.; Nasri, V.; Mould, J. Accounting for channeling and shielding effects for vapor cloud explosions. *J. Loss Prev. Process Ind.* **2017**, *50*, 205−220.
(31) Jallais, S.; Vyazmina, E.; Miller, D.; Thomas, J. K. Hydrogen jet vapor cloud explosion: a model for predicting blast size and application to risk assessment. *Process Saf. Prog.* **2018**, *37*, 397−410.
(32) Brunoro Ahumada, C.; Papadakis-Wood, F.-I.; Krishnan, P.; Yuan, S.; Quddus, N.; Mannan, M. S.; Wang, Q. Comparison of explosion models for detonation onset estimation in large-scale unconfined vapor clouds. *J. Loss Prev. Process Ind.* **2020**, *66*, 104165.
(33) Li, Y.; Ma, S. *Explosion Mechanics*; Science Press: Beijing, 1992.
(34) Shi, S.; Kang, J.; Wang, M.; Liu, Y.; li, X. *The Engineering Application of ANSYS/LS-DYNA in the Field of Explosion and Shock*; China Architecture Press: Beijing, 2011.
(35) *LS-DYNA Keyword User's Manual Volume II (Material Models)*, Version 971/Rev5. Livermore Software Technology Corporation, Inc: California, 2010.
(36) Wang, K.; Liu, Z.; Qian, X.; Li, M.; Huang, P. Comparative study on blast wave propagation of natural gas vapor cloud explosions in open space based on a full-scale experiment and PHAST. *Energy Fuels* **2016**, *30*, 6143−6152.
(37) Wang, J. *Simulation of Landmine Explosion using LS-DYNA3D Software: Benchmark Work of Simulation of Explosion in Soil and Air*; Defence science and technology organisation canberra: Australia, 2001.
(38) Qiang, H.; Sun, X.; Wang, G.; Huang, Q. Numerical simulation on steel box damage under internal explosion by smoothed particle hydrodynamics. *Baozha Yu Chongji* **2019**, *39*, 052201−0522019.
(39) Zhang, J.; Liang, Z.; Han, C. Collapse failure of directional crossing pipelines and the design of its protective devices. *Nat. Gas Ind.* **2015**, *35*, 91−96.
(40) Zhang, R.; Chen, G.; Zhang, H.; Chen, Q.; Yan, W. Engeering application of TNO multi-energy method in VCE simulation assessment. *Huanan Ligong Daxue Xuebao, Ziran Kexueban* **2006**, *34*, 109−114.
(41) Center for Chemical Process Safety, *Guideline for Chemical Process Quantitative Risk Analysis*. In 2nd ed. Wiley-AIChE, NewYork, 1999.
(42) Zhou, Z.; Zhou, J.; Jin, F.; Chen, H.; Xu, Y. Calculation and analysis of buried gas pipeline leakage. *Journal of PLA University of Science and Technology* **2017**, *18*, 243−248.
(43) Yan, Z.; Ye, Z.; Liu, P.; Cao, X. Collapsing process of high reinforced concrete chimney in blasting demolition. *Journal of Vibration and Shock* **2011**, *30*, 197−201.

https://doi.org/10.1021/acsomega.1c05332
ACS Omega 2021, 6, 34003−34020